



# Parametrizing the horizontal inhomogeneity of ice water content using CloudSat data products

Peter G. Hill<sup>a\*</sup>, Robin J. Hogan<sup>b</sup>, James Manners<sup>a</sup> and Jon C. Petch<sup>a</sup>

<sup>a</sup>Met Office, Exeter, UK

<sup>b</sup>Department of Meteorology, The University of Reading, Reading, UK

\*Correspondence to: Peter Hill, Met Office, FitzRoy Road, Exeter, EX1 3PB, UK. E-mail: peter.hill@metoffice.gov.uk

**In order to calculate unbiased microphysical and radiative quantities in the presence of a cloud it is necessary to know not only the mean water content, but also the distribution of this water content. This article describes a study of the in-cloud horizontal inhomogeneity of ice water content, based on CloudSat data. In particular, by focusing on the relations with variables which are already available in general circulation models (GCMs), a parametrization of inhomogeneity that is suitable for inclusion in GCM simulations is developed. Inhomogeneity is defined in terms of the fractional standard deviation (FSD), which is given by the standard deviation divided by the mean. The FSD of ice water content is found to increase with the horizontal scale over which it is calculated and also with the thickness of the layer. The connection to cloud fraction is more complicated; for small cloud fractions FSD increases as cloud fraction increases while FSD decreases sharply for overcast scenes. The relations to horizontal scale, layer thickness and cloud fraction are parametrized in a relatively simple equation. The performance of this parametrization is tested on an independent set of CloudSat data. The parametrization is shown to be a significant improvement on the assumption of a single-valued global FSD. Copyright © 2011 Royal Meteorological Society**

*Key Words:* Subgrid inhomogeneity, Ice clouds, CloudSat

*Received ...*

*Citation: ...*

## 1. Introduction

Many of the processes that are modelled in general circulation models (GCMs) are non-linear and the physical quantities on which these processes depend are often spatially variable at unresolved scales. Consequently, the process rate calculated using the gridbox mean value of such a variable is a biased estimate of the mean process rate within each gridbox. One such physical quantity is cloud water content. Pincus and Klein (2000) estimated that process rates calculated from gridbox mean water content values could have relative biases as large as 100%. Larson *et al.* (2001) showed that representing subgrid-scale water content variability is important for microphysics and thermodynamical processes. In particular they suggested that neglecting water content variability could lead to reduced autoconversion rates in GCMs. Subgrid-scale water

content variability is also important for radiative transfer calculations; the radiative effect of a cloud depends non-linearly on the cloud water content (e.g. Han *et al.* 1998). As a result, GCM radiative transfer calculations that use the mean cloud water content and assume that clouds are horizontally homogeneous do not give the correct domain mean radiative fluxes (e.g. Cahalan *et al.* 1994).

In the past decade, computationally efficient methods for representing the radiative effects of sub-grid cloud water content variability have been developed and tested (e.g. Pincus *et al.* 2003; Li *et al.* 2005; Shonk and Hogan 2008; Hill *et al.* 2011). Monte Carlo methods have also been suggested for representing the microphysical effects (Larson *et al.* 2005). While progress has been made towards representing the effects of subgrid-scale cloud variability in GCMs, it remains unclear how much subgrid-scale water content variability exists.

A number of articles have used observations to quantify horizontal cloud water variability (e.g. [Rossow \*et al.\* 2002](#); [Hogan and Illingworth 2003](#); [Oreopoulos and Cahalan 2005](#)). However, as highlighted in the review of [Shonk \*et al.\* \(2010\)](#), these published articles use different inhomogeneity parameters, observation sources, cloud types and space and time scales. As a consequence of this their results and conclusions are quite different and in some cases seem contradictory.

Studies that have considered radiative sensitivity to the magnitude of cloud water content variability suggest that it can have a significant impact. [Shonk and Hogan \(2010\)](#) estimated that the uncertainty in their estimate of a global mean variability parameter could change the global mean top of atmosphere (TOA) net radiation budget by 2–4  $\text{Wm}^{-2}$ . For a small systematic change to a globally varying inhomogeneity parameter, [Barker and Räisänen \(2005\)](#) estimated a smaller, but still significant change of 0.98  $\text{Wm}^{-2}$ , with larger changes at most latitudes. Although these values are small, they are significant when compared to the radiative forcing due to doubling  $\text{CO}_2$ , estimated to be 3.7  $\text{Wm}^{-2}$  ([Ramaswamy \*et al.\* 2001](#)). [Gu and Liou \(2006\)](#) considered the difference between two 5-year climate simulations. In one they scaled the optical depth of all clouds by a globally constant factor of 0.7 to account for water content inhomogeneity. In the other they used a globally varying climatological scaling factor for high-level clouds derived from International Satellite Cloud Climatology Project (ISCCP) data. They found significant differences, not only in the cloud albedo, which is directly affected by the change, but also in the cloud and precipitation fields.

[Barker \*et al.\* \(1996\)](#) found significantly different inhomogeneity parameters for stratocumulus and cumulus clouds, while [Oreopoulos and Cahalan \(2005\)](#) showed that cloud inhomogeneity varies with latitude. This implies that cloud water content variability depends on the meteorological regime, which means that a global mean inhomogeneity parameter will be a biased estimate of the inhomogeneity for different regimes. In a GCM simulation these biases could have feedback effects leading to further errors. GCMs do not generally predict meteorological regimes explicitly (e.g. they don't explicitly predict whether a cloud is stratocumulus or cumulus). Moreover using an inhomogeneity parameter that depends on location as in [Gu and Liou \(2006\)](#) means that the inhomogeneity parameter will be unable to respond to changes in climate. However, it may be possible to capture this dependence on regime using some of the variables predicted in a GCM.

In this article we describe water content variability in terms of the fractional standard deviation (FSD) of cloud water content. The FSD is simply the standard deviation divided by the mean. FSD was chosen as the inhomogeneity parameter because it accounts for the strong correlation (e.g. [Carlin \*et al.\* 2002](#)) between the mean and standard deviation of cloud water content, and it has been used in previous studies of water content variability (e.g. [Räisänen \*et al.\* 2004](#); [Shonk \*et al.\* 2010](#)). We are interested in in-cloud variability, so only include cloudy values (i.e. water content greater than zero) in the calculation of FSD. Moreover, we are interested only in the instantaneous spatial variability, not unresolved temporal changes in cloud water content, the radiative effects of which can be modelled by using output from a GCM cloud scheme (e.g. [Manners \*et al.\* 2009](#))

This study of cloud water content variability is based on CloudSat data. CloudSat ([Stephens \*et al.\* 2008](#)) is a polar orbiting satellite that carries a cloud radar and is part of the 'A-train', a constellation of satellites each carrying different instruments, orbiting the earth in sufficiently close proximity for their observations to be combined. The data product resolves cloud water content (the mass of liquid or ice water per unit volume of air) vertically and horizontally and thus is an excellent resource for the study of the magnitude of in-cloud water content variability. This article focuses on ice water content (IWC) variability as the retrieval is thought to be more accurate than that of liquid water. For further details on the CloudSat data used in this study, see Section 2.

This article describes the development of a parametrization for the FSD of ice water content, suitable for use in both numerical weather prediction (NWP) and climate models, based on CloudSat data. Section 2 consists of a brief description of the CloudSat data used in the study. In section 3 we perform a spectral analysis of the data, in order to inform the study of the dependence of water content variability on horizontal resolution, which is described in section 4. Section 5 discusses the sensitivity of FSD to the cloud fraction, while section 6 considers the effect of vertical resolution on the FSD. The final parametrization for use in GCMs is presented and tested in 7. Finally, conclusions are drawn and avenues for further work are highlighted in section 8.

## 2. CloudSat data

CloudSat was launched in April 2006 and data are available from June 2006. As one of five satellites in the sun-synchronous A-train, CloudSat orbits in close proximity to the Aqua satellite carrying the Moderate-Resolution Imaging Spectroradiometer (MODIS), which measures radiances. A number of CloudSat products have been developed, which combine observations from CloudSat, Aqua and other A-train satellites and are available from the CloudSat website (<http://www.cloudsat.cira.colostate.edu>). In particular, this study uses the 2B-CWC-RVOD (cloud water content, radar and visible optical depth) product, which combines CloudSat observations with MODIS radiance observations from the Aqua satellite in order to estimate the distribution of cloud water content within the atmosphere.

The algorithm used to produce this product is a modified version of that used to produce the equivalent radar only product that is described by [Austin \*et al.\* \(2009\)](#). We shall provide a brief description of the method for retrieving ice water content. A more extensive description is available from the CloudSat website.

The retrieval assumes that ice particles are spheres with a log-normal particle size distribution (PSD). The PSD has three parameters: the geometric mean particle diameter, the distribution width parameter and the total particle number concentration. A priori values for the first two parameters are temperature dependent. The a priori particle concentration is more complex (see [Austin \*et al.\* \(2009\)](#) for details). Optimal parameter values are obtained by using the PSD to forward model the extinction and backscatter, then comparing to observations. Once the optimal parameters have been calculated, ice water content is calculated by integrating over the PSD, assuming the ice particles have the density of solid ice ( $0.917 \text{ kgm}^{-3}$ ). Separate retrievals

are performed for liquid and ice; ice properties are used at temperatures less than  $-20^{\circ}\text{C}$ , liquid at temperatures larger than  $0^{\circ}\text{C}$  and a linear combination of the two at intermediate temperatures.

Each of the 2B-CWC-RVOD profiles measures 1.7 km along track and 1.3 km across track and divides the atmosphere into 125 vertical layers each of which is 240 m thick. At this horizontal scale, almost all of the cloud water content variability is captured (Oreopoulos and Davies 1998). The largest length scales used in this study consist of 500 CloudSat profiles, which corresponds to 850 km. As a new CloudSat profile is observed every 0.16 seconds, 850 km of data is observed in only 80 seconds and any variability is approximately instantaneous, an advantage over ground-based studies where changes in time are assumed to be due to changes in space advected over the site (e.g. Hogan and Illingworth 2003).

The cloud profiling radar on board CloudSat operates at 94 GHz. At this frequency radars suffer virtually no attenuation by ice water (Hogan and Illingworth 1999). However, in liquid clouds, drizzle droplets can dominate the radar reflectivity factor while containing negligible liquid water and thus the radar reflectivity factor is not a good indicator of the liquid water content (Fox and Illingworth 1997). For this reason, CloudSat estimates of ice water content are expected to be more accurate than those of liquid water content. Hence we focus on the FSD of ice water content. It should be noted that this ice water content includes all frozen hydrometeors. Thus the results presented here are not necessarily applicable to ice particles that have been split into multiple categories, such as ‘‘precipitating’’ and ‘‘suspended’’.

This study uses data from two separate arbitrarily chosen periods. Initially we use data observed between 22nd December 2007 and 10th January 2008, a total of 9,752,539 CloudSat profiles, and over a billion values of ice water content. As the satellite is polar orbiting, this includes observations from all latitudes and longitudes and should be representative of the whole CloudSat data set. Nevertheless, to check that it is indeed representative, we test the parametrization on data observed between 15th June and 25th June 2006 (5,006,028 profiles and over 500 million water content observations).

### 3. Spectral Analysis

A number of metrics have been used to study the statistical properties of clouds (e.g. Marshak *et al.* 1997). In this section we use one such technique, spectral analysis, to study CloudSat ice water content. We chose this metric as it is most widely used in the existing literature (e.g. Cahalan and Joseph 1989; Lewis *et al.* 2004; Davis *et al.* 1999) and thus allows us to confirm that the spatial statistical properties of the CloudSat ice water content are consistent with other observation sources. This spectral analysis complements the following section, which considers how the FSD changes with horizontal domain size.

Many previous studies have observed that for scales between metres and tens of kilometres, the wavenumber spectrum of cloud water content approximately follows a  $-5/3$  power law (e.g. Davis *et al.* 1996; King *et al.* 1981). However, this  $-5/3$  power law is not observed universally. For example, using ground-based radar observations of a cirrus cloud, Hogan and Kew (2005) found that for scales

less than 50 km, the power spectrum of the natural logarithm of ice water content appears to obey a  $-5/3$  power law at cloud top, with the spectra becoming steeper with depth into the cloud, obtaining values as low as  $-3.5$  in some cases. This is thought to be due to the effects of wind shear. For scales larger than 50 km they find that the spectra are flat. Lewis *et al.* (2004) calculated spectra for LandSat observations of marine boundary layer clouds. They considered 12 overcast and 12 partially cloudy scenes and found that the spectrum of liquid water path obeyed a  $-5/3$  power law for overcast scenes. For the partially cloudy scenes the spectra displayed more scene to scene variability with the average spectrum following a  $-1$  power law.

We calculated the mean ice water content spectrum for isolated clouds of various sizes, the smallest containing 8 CloudSat cells and the largest containing 128 cells (i.e. 13.6 km and 217.6 km long respectively). These spectra were produced as follows. Each layer of the CloudSat data was divided into individual clouds, separated by at least one clear-sky cell. The ice water content for each cloud was divided by the mean ice water content for that cloud and the spectrum for the resulting normalised ice water content was calculated. The spectra for individual clouds of the same size were then averaged together and multiplied by the size of the cloud (i.e. the number of cells in the cloud). By Parseval’s theorem, the integral of the resulting mean spectrum for a given cloud size is equal to the mean fractional variance (FVAR) for clouds of that size, where the FVAR of a cloud is defined as the square of the FSD of that cloud. (Note however, that as the square is non-linear, the mean FVAR is not equal to the square of the mean FSD.) These spectra are shown in Figure 1 below.

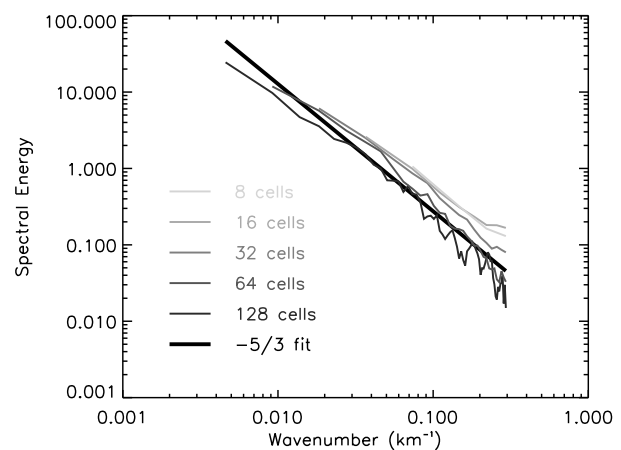


**Figure 1.** Mean spectra for clouds of fixed size, ranging from 8 to 128 CloudSat cells (thin lines). For comparison, the thick black line obeys a  $-5/3$  power law.

Figure 1 shows several interesting features. The spectrum for each cloud size appears to approximately obey a  $-5/3$  power law, as shown by the thick black line. This is consistent with the existing literature, as described at the beginning of this section. While the spectra obey a  $-5/3$  power law for all cloud sizes, the values of the spectra decrease for larger clouds. This implies that the FVAR per unit length of a small cloud is larger on average than that of a larger cloud. Despite this, the integral under the spectrum

increases for larger clouds, because we integrate over a larger horizontal scale.

As the mean spectrum,  $E$  for a cloud of length  $x$  can be approximated by a power law of the form

$$E = A(x)k^{-5/3}, \quad (1)$$

where  $k$  is the wavelength, the mean FVAR for a cloud of length  $x$  can be calculated by integrating under the spectrum as follows

$$\text{FVAR} = \int_{1/x}^{1/x_1} E(k)dk = A(x)(x^{2/3} - x_1^{2/3}). \quad (2)$$

The upper limit of the integral,  $1/x_1$  corresponds to the maximum wavenumber for which the spectrum is defined. This means that  $x_1$  is equal to the resolution of the data, which in the case of the 2B-CWC-RVOD data used here equals 1.7 km.

Water content spectra have been observed to follow power laws down to scales as small as 3 m (King *et al.* 1981). This suggests that the spectra observed in Figure 1 can be extrapolated to smaller scales. In this case, the mean FVAR for a cloud of length  $x$  will simplify to

$$\text{FVAR} = A(x)x^{2/3}. \quad (3)$$

Note however, that while this is a prediction of the actual FVAR, to ensure the best comparison to the CloudSat data we must include the  $x_1$  in order to exclude the variability that is unresolved in the data.

In our spectral analysis, we have considered how ice water content variability changes with cloud size. However, the sizes of individual clouds are not predicted in GCMs, which in general simply predict the cloud fraction within a gridbox. Consequently the observed relationship between variability and cloud size cannot be used as a basis for the parametrization.

#### 4. Horizontal scale

In this section we consider how the FSD of ice water content changes with the scale of the domain over which it is calculated. For ground-based cloud radar data, Hogan and Illingworth (2003) found that, for overcast gridboxes, the FVAR of ice water content was proportional to the size of the gridboxes to the power of 0.3 for scales up to 60 km, but that it grows no further for larger gridboxes.

To calculate the IWC FSD for a given domain size, each layer of the data is sub-divided horizontally into adjacent 'gridboxes' each containing the same number of CloudSat cells. For each gridbox that contains more than one cloudy cell the FSD is calculated. Figure 2 shows the mean FSD of both ice water content and ice water path (calculated by summing the ice water content in a column), calculated for gridboxes ranging from 4 to 500 profiles (6.8 to 850 km) in size. The FSD rises sharply with gridbox size at smaller scales, then levels off at larger scales. Note that the FSD for water path is larger than that for water content. This contradicts the suggestion by Shonk *et al.* (2010) that the FSD for water content was larger. This relationship is considered in more detail in section 6, where we consider the effect of the layer thickness on the inhomogeneity.

The trend of the FSD can be explained by the results of the spectral analysis. The FSD increases with gridbox size

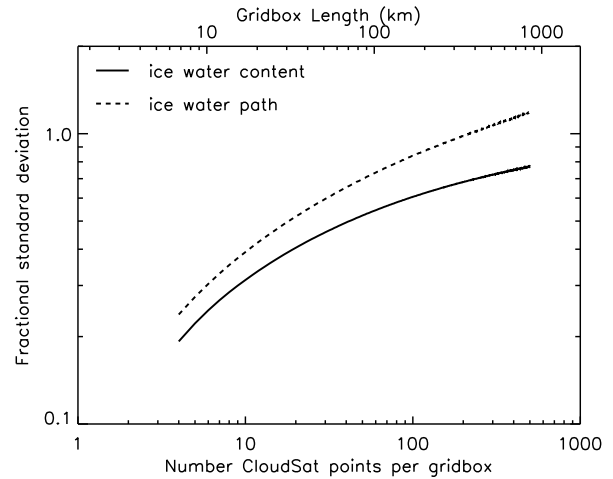


**Figure 2.** Mean FSD of ice water content (solid line) and ice water path (dashed line) when data is divided into horizontal boxes containing the given number of CloudSat profiles.

because as the gridbox size is increased, the gridbox may contain larger clouds, which have larger values of FSD. The slope decreases with gridbox size because the rate at which the FSD rises with cloud size decreases and larger clouds occur less frequently.

Figure 3 again shows how the FSD of ice water content increases with gridbox size (solid black line), this time with vertical bars that show the standard deviation of the FSD for a selection of the gridbox sizes. The dashed line shows the case when we include only overcast gridboxes, in which case the results are similar to those of Hogan and Illingworth (2003), who also considered only overcast gridboxes. Note that the standard deviation of the FSD is much smaller when only overcast gridboxes are included. This implies that a considerable amount of the variability of the FSD is due to the variability in cloud fractions, which suggests there is a significant relationship between FSD and cloud fraction, which is considered in more detail in Section 5. As the FSD for overcast gridboxes is less variable, we shall begin by parametrizing this and then extend the parametrization to capture some of the extra variability that is introduced when different cloud fractions are considered.

An overcast gridbox can only contain clouds that are larger than or equal to that gridbox in size. Thus the mean FSD for an overcast gridbox of size  $x$  can be calculated by summing the contributions to the FSD for each cloud size, approximately equal to the square root of equation 2, and weighting by the likelihood of sampling a cloud of that size,

$$\text{FSD} = \sqrt{x^{2/3} - x_1^{2/3}} \sum_{z=x}^{\infty} \sqrt{A(z)}W(z), \quad (4)$$

where  $W(z)$  is the likelihood of an overcast gridbox of size  $x$  being a sample from a cloud of size  $z$ . Using a gradient-expansion algorithm to compute a non-linear least squares fit, we can approximate the sum by a combination of power laws, resulting in the following parametrization for the FSD of an overcast gridbox of size  $x$  km,

$$\text{FSD} = 0.13 \sqrt{x^{2/3} - 1.41} \left[ (0.016x)^{1.10} + 1 \right]^{-0.26}. \quad (5)$$

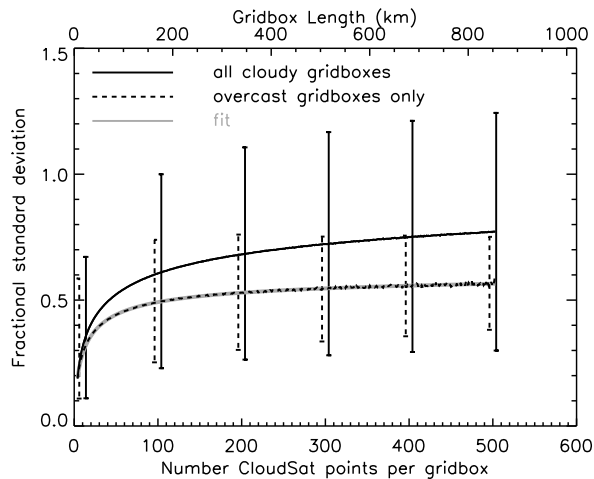


**Figure 3.** Mean FSD of ice water content as a function of gridbox size for all data (solid line) and only those gridboxes that are overcast (dashed line). The vertical bars show the standard deviation of the FSD for the given gridbox size. The grey line shows the FSD given by equation 5.

The FSD predicted by equation 5 is shown by the grey line in Figure 3 and is an excellent fit to the mean observed FSD. Note that the  $-1.41$  term corresponds to putting the CloudSat resolution as the value of  $x_1$  and is only necessary when comparing to the observed data, to account for the unresolved variability.

## 5. Variability as a function of cloud fraction

According to Cahalan (1994), in the case of California marine stratocumulus, the liquid water content variance increases as the cloud fraction increases. This could perhaps be explained by the horizontal scale dependence discussed in the previous section. By contrast, Oreopoulos and Cahalan (2005) found no strong relationship between cloud fraction and inhomogeneity, except for cloud fractions greater than 0.9, when clouds become considerably more homogeneous. In this section, we investigate the relationship between FSD and cloud fraction and attempt to explain these apparently contradictory results.

Figure 4 shows the mean FSD when gridboxes with cloud fraction within a given range are binned together. Values for gridboxes containing 25, 50, 100 and 200 CloudSat cells are shown. For all gridbox sizes, FSD initially increases with cloud fraction, then remains fairly constant, before dropping off sharply if the gridbox is overcast. As the gridbox size is increased, the cloud fraction at which the FSD no longer increases gets smaller. This suggests that the observed increase in FSD with cloud fraction is related to cloud size rather than cloud fraction.

Assuming that the CloudSat resolution is sufficient to resolve cloud edges, an overcast gridbox contains only a single cloud and in almost all cases excludes the edges of that cloud. In theory, either or both of these could lead to the steep decrease in FSD that is observed as cloud fractions approach one. A gridbox containing a single cloud may have a lower in-cloud FSD than one containing multiple clouds, which includes contributions from both internal cloud variability and the variance in mean water content between different clouds (cf. Figure 8). Cloud edges often contain lower values of liquid water content than the rest of

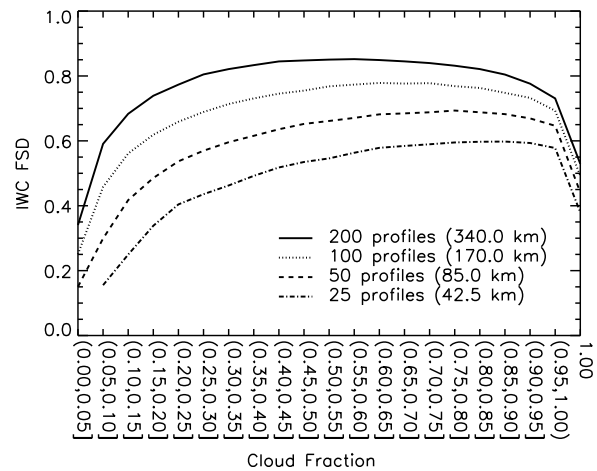


**Figure 4.** Fractional standard deviation of ice water content (IWC FSD) as a function of cloud fraction for gridboxes containing 200, 100, 50, and 25 CloudSat cells (solid, dotted, dashed and dot-dashed lines respectively).

the cloud, and as a result have the effect of both increasing the variability of water content in the cloud and decreasing the mean water content of the cloud. Both of these lead to larger values of FSD.

Alongside the FSD for all gridboxes, Figure 5 shows the FSD for those gridboxes that contain exactly one cloud, but not necessarily the entire cloud (where a gridbox contains one cloud if the cloudy cells are not separated by any clear cells). Also shown is the FSD for gridboxes that contain exactly one cloud and both cloud edges (where the edges are defined as the single cloudy cells at either end of the cloud). Data for gridboxes containing 50 cells are shown. It is clear that the drop in FSD as cloud fraction nears one is due to the fact that overcast gridboxes tend not to include cloud edges.

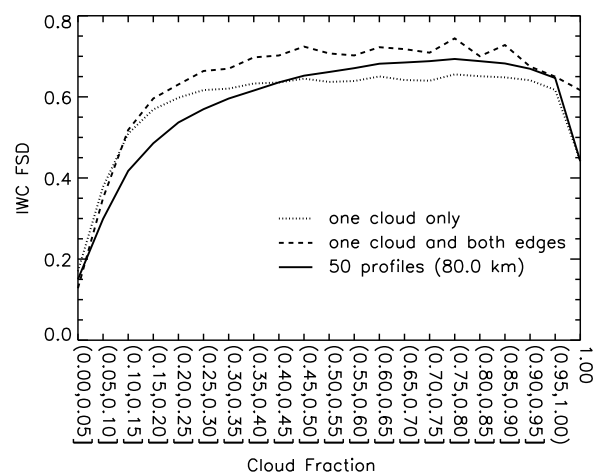


**Figure 5.** Fractional standard deviation of ice water content (IWC FSD) as a function of cloud fraction for gridboxes containing 50 cells. Solid lines show the FSD for all gridboxes. Dotted lines show the FSD for those gridboxes that contain one cloud only. Dashed lines show the FSD for those gridboxes that contain only one cloud and contain all of this cloud.

Equation 5 gives the FSD only for a cloud fraction of one. In developing a parametrization applicable to smaller

cloud fractions, we start by replacing the dependence on gridbox size ( $x$ ) with a dependence on cloud extent ( $xc$ ) (i.e. the gridbox size multiplied by the cloud fraction). However, the resulting FSD is an underestimate for cloud fractions smaller than one. The four thin black lines in Figure 6 show the ratio of the observed mean FSD to this predicted FSD, for the same 20 cloud fractions and four gridboxes sizes in Figure 4. Note that we do not include overcast scenes, for which equation 5 is a good estimate. These ratios are reasonably similar for all gridbox sizes, except for small cloud fractions, where the FSD is already small, so a large difference in ratio has less impact. Since the ratios are similar, we average across the four gridbox sizes, as shown by the light grey line and then fit a linear function of cloud fraction to this average, as shown by the thick dark grey line.

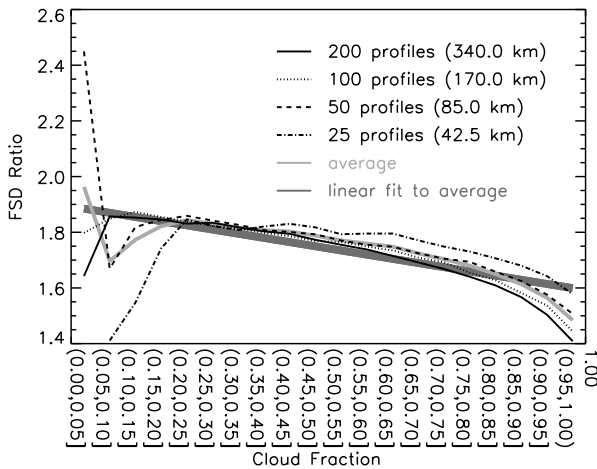


**Figure 6.** Ratio of observed ice water content fractional standard deviation (FSD) and the FSD predicted by equation 5 as a function of cloud fraction. Note that we use the cloud extent instead of the gridbox size in equation 5. The thin black lines correspond to the observed relationship for the different gridbox sizes. The light grey line shows the average relationship for these gridbox sizes and the dark grey line shows a linear fit to this average relationship.

Combining the average ratio estimated from Figure 6 and the FSD based on cloud extent gives the following equation for the FSD for a partially cloudy gridbox.

$$\text{FSD} = (0.25 - 0.04c) \sqrt{(xc)^{2/3} - 1.41} \left[ (0.016xc)^{1.10} + 1 \right]^{-0.26} \quad (6)$$

where  $c$  is the cloud fraction. The FSD predicted by this equation is shown in Figure 7. The equation captures the FSD pattern well, though the slight decrease in FSD as cloud fractions approach one, which is particularly evident for the large gridboxes, is not captured by the parametrization. As a result the FSD for cloud fractions around 0.9 is overestimated. For the smallest gridboxes, the FSD for very small cloud fractions is overestimated. However, for other gridbox sizes the initial increase in FSD with cloud fraction is very well predicted and for intermediate cloud fractions the parametrization errors are small. Despite being relatively simple, the parametrization provides a very good estimate of the complex relationship between IWC variability and cloud fraction at all gridbox sizes.

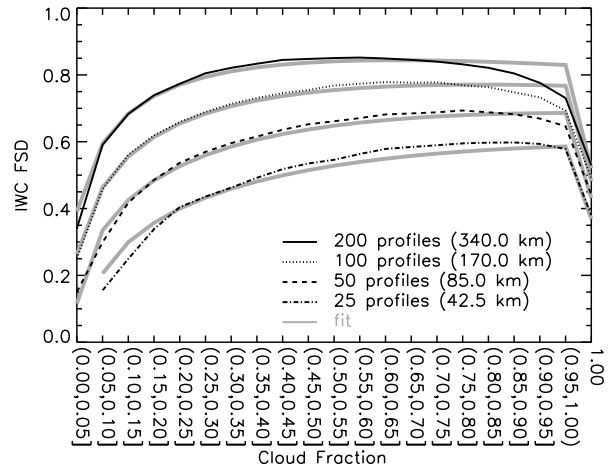


**Figure 7.** Fractional standard deviation of ice water content (IWC FSD) as a function of cloud fraction. Black lines are as in Figure 4. Grey lines show the FSD predicted by equation 6.

## 6. Vertical layer thickness

Figure 2 shows that the FSD of ice water path is larger than that of ice water content, which suggests that the FSD increases as vertical resolution decreases. This section considers the relationship between FSD and vertical layer thickness in more detail.

To determine the sensitivity of FSD to vertical scales, IWC values are averaged in the vertical to create thicker layers. For example, after the original data, the next highest resolution data was calculated by summing the IWC in adjacent layers to create a profile containing 124 overlapping vertical layers each of which is 480 m thick (recall the original data has 125 layers, each of which is 240 m thick).

Figure 8 shows the mean FSD calculated for layers of the given thickness, for two different horizontal gridbox sizes, containing 200 and 25 CloudSat cells. The solid lines include all data and show that the FSD increases as layer thickness increases. The increase is most rapid for the thinnest layers, which correspond to the vertical resolutions that are likely to be used in GCMs.

The increase in FSD as the layer thickness increases can be explained as follows. Consider a gridbox containing multiple layers, each of which contains  $n$  cloudy cells, covering a fraction of the gridbox. Assume that the clouds are horizontally homogeneous and the water content in each cloudy cell equals  $x$ . Thus the FSD in any layer equals zero. Now sum the water contents in the vertical. If the same  $n$  cells are cloudy in each layer (i.e. the clouds are exactly overlapped), then the integrated water content in each column will be the same and the FSD will be zero. However if not, then the columns would contain different integrated water content and FSD will be non-zero. That is, the integrated FSD would be larger than that in any layer because the integrated FSD is accounting for apparent in-cloud inhomogeneity that is in fact simply due to the vertical resolution being insufficient to resolve cloud boundaries.

The dashed lines in Figure 8 show how the FSD changes with layer thickness for gridboxes that contain one cloud whose layers are exactly overlapped (i.e. the vertically integrated cloud fraction is identical to the cloud

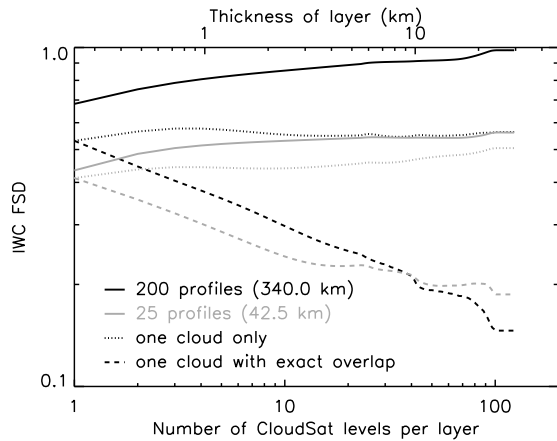


**Figure 8.** Mean fractional standard deviation of ice water content (IWC FSD) for given vertical resolution. The solid lines show the mean FSD when no restrictions are applied to the data, the dotted lines show the mean FSD for those gridboxes that contain only one cloud (i.e. no breaks between cloudy cells) and the dashed lines show the FSD for those gridboxes that contain only one cloud where exactly the same cells contain cloud in each layer of the original data. The black lines correspond to gridboxes containing 200 cells and the grey lines to gridboxes containing 25 cells.

fraction in each layer). For these gridboxes, the FSD does not need to account for any unresolved cloud structure. Hence the FSD decreases as layer thickness increases. This is the behaviour predicted by [Shonk \*et al.\* \(2010\)](#), who suggested that this is because in-cloud water content decorrelates as the distance between layers increases (e.g. [Barker and Räisänen 2005](#); [Hogan and Illingworth 2003](#)), which has the effect of smoothing the vertical average.

The FSD for those gridboxes that contain exactly one cloud, with no restriction on overlap between cloud in different layers, is shown by the dotted lines in [Figure 8](#). Now the FSD has to account for some unresolved cloud structure. As the layer thickness increases, the amount of unresolved structure increases. The competing effects of the unresolved cloud structure and the smoothing effect of decorrelating water content lead to a FSD that generally increases slightly with layer thickness.

If no restrictions are placed on the gridboxes (other than that they contain some cloud), then there may be multiple clouds in the gridbox and as the layer thickness increases, there may be a great deal of unresolved cloud structure. This means that the FSD increases significantly as layer thickness increases, as shown by the solid lines in [Figure 8](#).

[Figure 8](#) suggests that FSD of ice water content is quite sensitive to vertical resolution and that it is worthwhile including a vertical resolution dependence in any parametrization. For simplicity, the parametrization is restricted to layers that are thinner than 2.4 km (i.e. contain less than 10 CloudSat layers). Beyond this scale, the relationship between FSD and layer thickness cannot be accurately described with a simple equation. Moreover, the relevant layers in current GCMs (i.e. the layers that contain clouds) are generally thinner than 2.4 km.

The relevant part of [Figure 8](#) is shown again in [Figure 9](#) (note that it is no longer in log-log space). The broken lines show the relationship between FSD and layer thickness,

which appears to be best described by a power law. The dark grey lines show the mean FSD given by [equation 6](#). Neither of the dark grey lines show any significant change with increasing thickness, which implies that the thickness dependence is independent of this equation. Thus we assume that we can predict the FSD for a single layer exactly and simply consider how the relationship between this FSD and the multi-layer FSD changes with increasing layer thickness. Letting  $\Delta z$  denote the layer thickness (in km) and  $A$  denote the FSD for a single layer, a least square error fit gives

$$\text{FSD} = A \left( \frac{\Delta z}{0.24} \right)^{0.11} \quad (7)$$

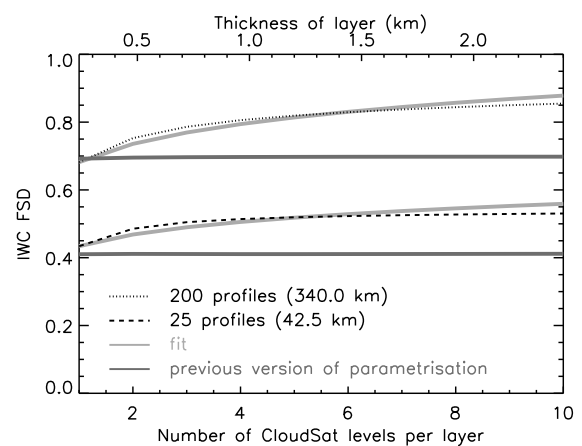


**Figure 9.** Mean fractional standard deviation of ice water content (IWC FSD) for vertical resolution between 240 m and 2.4 km. For gridboxes of length 340 km (dotted line) and 42.5 km (dashed line). The dark grey lines show the mean FSD predicted by [equation 6](#), which does not include any dependence on layer thickness. The light grey lines show the FSD given by [equation 7](#), where the value of  $A$  is chosen so that the equation gives the observed value of FSD for individual CloudSat layers.

## 7. Parametrization

We have seen that the mean in-cloud FSD depends on the scale over which it is calculated (both horizontally and vertically) and cloud fraction. The remainder of this article illustrates how these relationships can be combined into a single parametrization and describes the results of testing this parametrization.

The mean FSD for a gridbox of horizontal length  $x$  km and thickness  $\Delta z$  km is obtained by combining [equations 5 and 7](#) to get [equation 8](#), where  $c$  is the cloud fraction. Note that  $x_1$  is again equal to the minimum resolved scale, and for the purpose of comparing this parametrization to CloudSat observations is set to 1.7 km. However when this parametrization is implemented in a GCM,  $x_1$  should be set to zero.

### 7.1. Comparing observed FSD to modelled FSD

The parametrization defined by [equation 8](#) is tested on several days of CloudSat data from Summer 2006. These data are independent of the CloudSat data that were used

$$\text{FSD} = \begin{cases} (0.29 - 0.05c)\sqrt{(xc)^{2/3} - 1.41} \left[ (0.016xc)^{1.10} + 1 \right]^{-0.26} (\Delta z^{0.11}) & \text{if } c < 1; \\ 0.15\sqrt{x^{2/3} - 1.41} \left[ (0.016x)^{1.10} + 1 \right]^{-0.26} (\Delta z^{0.11}) & \text{if } c = 1. \end{cases} \quad (8)$$

to develop the parametrization. The data were divided into gridboxes of size 200, 100, 50 and 25 km (which corresponds to gridboxes containing 117, 59, 29 and 15 CloudSat profiles respectively) and thickness from 240 m to 2.4 km in 240 m increments (which corresponds to vertically averaging between 1 and 10 CloudSat layers). For each cloudy gridbox, the observed FSD and parametrized FSD were calculated. These were then used to calculate the parametrization bias (i.e. the mean difference between the FSD predicted by the parametrization and the observed FSD), shown in Figure 10 and the mean absolute error (the mean of the absolute value of the difference between the FSD predicted by the parametrization and the observed FSD) of the parametrization, shown in Figure 11. To put these values into context, the bias and mean absolute error for a constant FSD equal to 0.75 are also shown. This is the global mean FSD for all cloud types estimated by Shonk *et al.* (2010) based on a review of the existing literature.

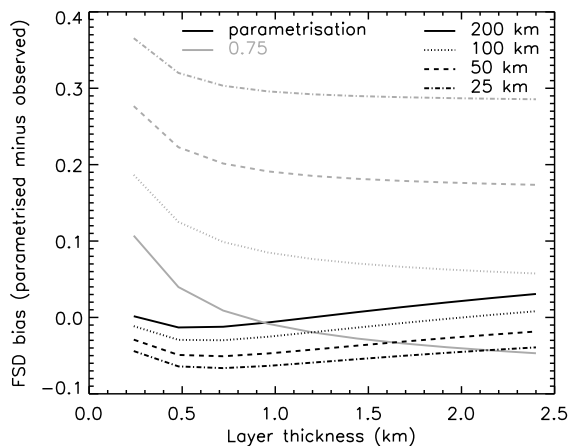


**Figure 10.** Mean difference between the fractional standard deviation (FSD) of ice water content given by equation 8 and the observed FSD, for layers between 240 m and 2.4 km in thickness and gridbox sizes of 200 (solid), 100 (dotted), 50 (dashed) and 25 (dot-dashed) km.

The bias of the FSD predicted by the parametrization is small for all gridbox sizes and layer thicknesses. The behaviour of this bias can be understood by considering the individual components of the parametrization. The relationship between FSD bias and layer thickness is similar for all four gridbox sizes and is the same as that for the thickness parametrization shown in Figure 9. The relationship between FSD bias and gridbox size is consistent with that shown in Figure 7. The constant FSD is a good estimate of the mean FSD for gridboxes that are 200 km in length, but overestimates the observed FSD for smaller gridboxes and has larger biases than the parametrization for all gridbox sizes.

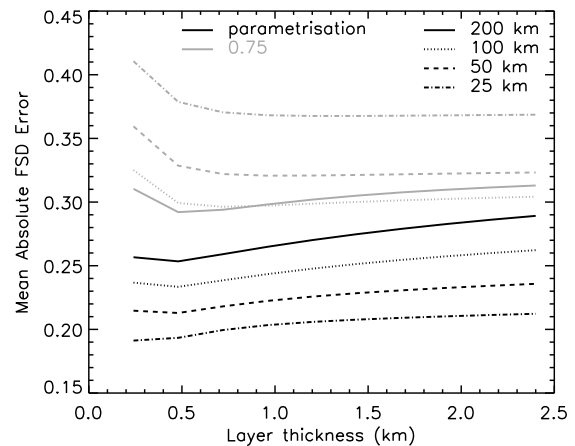


**Figure 11.** Mean absolute difference between the fractional standard deviation (FSD) of ice water content given by equation 8 and the observed FSD, expressed as a percentage of the mean observed FSD. Layers range from 240 m to 2.4 km in thickness and gridbox sizes are 200 (solid), 100 (dotted), 50 (dashed) and 25 (dot-dashed) km.

The mean absolute errors of the FSD predicted by the parametrization are shown in Figure 11. These errors increase with gridbox thickness and length. The largest error is approximately 0.29 and corresponds to gridboxes that are 2.4 km thick and 200 km long. The mean absolute errors for the parametrization are smaller than those obtained from the single FSD value for all gridbox sizes and thicknesses. Of particular note is the improvement for the gridboxes that are 200 km long and 1.0 km thick. Here the biases for both the parametrization and 0.75 are approximately zero. However, due to the cloud fraction dependence in the parametrization, the mean absolute error for the parametrization is significantly smaller than that for FSD=0.75.

The information shown in these Figures is summarised in Table I, which shows mean values across all the horizontal and vertical scales included in Figures 10 and 11. To add further context we also include the statistics for the mean FSD, calculated by averaging the mean FSD for each of the resolutions shown in Figures 10 and 11. This is unbiased when all the data is combined, but biased for any individual resolution. The bias row shows the mean error of all biases shown in Figure 10, which is zero by definition for the mean. The mean absolute bias row shows the mean of the absolute value of the the biases shown in Figure 10 and the mean absolute error shows the mean of the absolute errors shown in Figure 11. The parametrization performs better than both the unbiased FSD value and the control FSD.

The mean absolute FSD error can be split into four components. Some of the error is due to the relationships

	Control (0.75)	Mean (0.60)	Param
Bias	0.15	0.00	-0.02
Mean absolute bias	0.16	0.11	0.03
Mean absolute error	0.33	0.28	0.24

Table I. Mean statistics for all the data shown in Figures 10 and 11.

that are included in the parametrization being in error. This corresponds to the errors that arose when fitting equations to the observed trends. There is also a component due to a FSD dependence on variables that are not included in the parametrization. For example Hogan and Illingworth (2003) found a dependence on wind shear, which is not included in this parametrization, due to a lack of reliable global wind speed data to compare to the ice water content observations. The third component of the mean absolute error is the sampling error introduced when the observed FSD is calculated. This decreases as the gridbox size increases. This could be reduced by using higher resolution observations. The final component of the error is due to unpredictable variability of FSD; Hogan and Illingworth (2003) observed that even within a single cloud, the horizontal inhomogeneity varies significantly.

## 8. Summary

This article describes a study of ice water content variability using combined CloudSat and MODIS observations. Ice water content variability is considered in terms of the fractional standard deviation (FSD); the standard deviation divided by the mean. Results show that FSD increases as the horizontal scale over which it is calculated increases and when water content is averaged over larger vertical scales. A nonlinear dependence on cloud fraction was also identified; FSD was seen to increase with cloud fraction for small cloud fractions, while the mean FSD for overcast gridboxes was found to be significantly smaller than that for gridboxes with large cloud fractions. This decline in FSD was shown to be a result of overcast gridboxes excluding cloud edges. These relationships have been included in a relatively simple parametrization of ice water content, suitable for use in a GCM.

The performance of the new parametrization was tested using data taken from a different period in time. For the horizontal and vertical resolutions considered, the magnitude of the parametrization bias was shown to be less than 0.07. Mean absolute errors were found to be larger, but significantly smaller than those arising from the use of a single global FSD. The size of these mean absolute errors suggests that the parametrization could be developed further, either by using a function that better fits the relationships considered in this paper, or by including the effect of other variables (e.g. wind shear) on the FSD.

In future work, this parametrization will be implemented in the UK Met Office Unified Model (MetUM) and tested in both NWP and climate simulations. Results of these tests should indicate how much benefit there would be in further developing the parametrization, for example by linking FSD to meteorological regime.

In many GCMs ice particles are split into two or more categories (often described as ice and snow). However, there is no such split in either the CloudSat data product or the MetUM. Consequently, there is no such split in the parametrization described in this paper. When this

parametrization is included in other GCMs, care should be taken to ensure that it is applied to the *total* ice content. This may be more challenging for those GCMs which have a diagnostic ice category.

The existing parametrization is for ice water content only. Liquid water content variability is equally important and it is not clear whether it is significantly different. Using MODIS data, Oreopoulos and Cahalan (2005) found similar variability in ice and liquid clouds. On the other hand, Shonk and Hogan (2008) found that ice clouds exhibit more water content variability than liquid clouds. It would be informative to compare this parametrization to observations of liquid water content variability.

## Acknowledgements

CloudSat data were obtained from the CloudSat Data Processing Center (<http://cloudsat.cira.colostate.edu>). We'd like to thank two anonymous reviewers for their constructive and insightful comments.

## References

- Austin RT, Heymsfield AJ, Stephens GL. 2009. Retrieval of ice cloud microphysical parameters using the cloudsat millimeter-wave radar and temperature. *J. Geophys. Res.* **114**(D00A23).
- Barker HW, Räisänen P. 2005. Radiative sensitivities for cloud structural properties that are unresolved by conventional GCMs. *Q. J. Roy. Meteorol. Soc.* **131**: 3103–3122.
- Barker HW, Wielicki BA, Parker L. 1996. A parameterization for computing grid-averaged solar fluxes for inhomogeneous marine boundary layer clouds. Part II: Validation using satellite data. *J. Atmos. Sci.* **53**(16): 2304–2316.
- Cahalan RF. 1994. Bounded cascade clouds: albedo and effective thickness. *Nonlinear Processes in Geophysics* **1**(2/3): 156–167.
- Cahalan RF, Joseph JH. 1989. Fractal statistics of cloud fields. *Monthly Weather Review* **117**(2): 261–272.
- Cahalan RF, Ridgway W, Wiscombe WJ, Bell TL, Snider JB. 1994. The albedo of fractal stratocumulus clouds. *J. Atmos. Sci.* **51**(16): 2,434–2,455.
- Carlin B, Fu Q, Lohmann U, Mace GG, Sassen K, Comstock JW. 2002. High-cloud horizontal inhomogeneity and solar albedo bias. *J. Climate* **15**(17): 2321–2339.
- Davis A, Marshak A, Wiscombe W, Cahalan R. 1996. Scale invariance of liquid water distributions in marine stratocumulus. Part I: Spectral properties and stationarity issues. *J. Atmos. Sci.* **53**(11): 1538–1558.
- Davis AB, Marshak A, Gerber H, Wiscombe WJ. 1999. Horizontal structure of marine boundary layer clouds from centimeter to kilometer scales. *J. Geophys. Res.* **104**(D6): 6123–6144.
- Fox NI, Illingworth AJ. 1997. The potential of a spaceborne cloud radar for the detection of stratocumulus clouds. *Journal of Applied Meteorology* **36**(6): 676–687.
- Gu Y, Liou KN. 2006. Cirrus cloud horizontal and vertical inhomogeneity effects in a GCM. *Meteorol Atmos Phys* **91**: 223–235.
- Han Q, Rossow WB, Chou J, Welch RM. 1998. Global survey of the relationships of cloud albedo and liquid water path with droplet size using ISCCP. *J. Climate* **11**(7): 1516–1528.
- Hill PG, Manners J, Petch JC. 2011. Reducing noise associated with the Monte Carlo Independent Column Approximation for weather forecasting models. *Q. J. Roy. Meteorol. Soc.* **137**: 219–228.
- Hogan RJ, Illingworth AJ. 1999. The potential of spaceborne dual-wavelength radar to make global measurements of cirrus clouds. *Journal of Atmospheric and Oceanic Technology* **16**(5): 518–531.

- Hogan RJ, Illingworth AJ. 2003. Parameterizing ice cloud inhomogeneity and the overlap of inhomogeneities using cloud radar data. *J. Atm. Sci.* **60**(5): 756–767.
- Hogan RJ, Kew SF. 2005. A 3D stochastic cloud model for investigating the radiative properties of inhomogeneous cirrus clouds. *Q. J. Roy. Meteorol. Soc.* **131**(611): 2585–2608.
- King WD, Maher CT, Hepburn GA. 1981. Further performance tests on the CSIRO liquid water probe. *J. Appl. Met.* **20**(2): 195–202.
- Larson VE, Golaz JC, Jiang H, Cotton WR. 2005. Supplying local microphysics parameterizations with information about subgrid variability: Latin hypercube sampling. *Journal of the Atmospheric Sciences* **62**(11): 4010–4026.
- Larson VE, Wood R, Field PR, Golaz JC, Haar THV, Cotton WR. 2001. Systematic biases in the microphysics and thermodynamics of numerical models that ignore subgrid-scale variability. *J. Atm. Sci.* **58**(9): 1117–1128.
- Lewis GM, Austin PH, Szczodrak M. 2004. Spatial statistics of marine boundary layer clouds. *J. Geophys. Res.* **109**(D04104).
- Li J, Dobbie S, Räisänen P, Min Q. 2005. Accounting for unresolved clouds in a 1-D solar radiative transfer model. *Q. J. Roy. Meteorol. Soc.* **131**: 1607–1629.
- Manners J, Thelen JC, Petch J, Hill P, Edwards JM. 2009. Two fast radiative transfer methods to improve the temporal sampling of clouds in numerical weather prediction and climate models. *Q. J. Roy. Meteorol. Soc.* **135**: 457–468.
- Marshak A, Davis A, Wiscombe W, Cahalan R. 1997. Scale invariance of liquid water distributions in marine stratocumulus. Part II: Multifractal properties and intermittency issues. *J. Atm. Sci.* **54**(11): 1423–1444.
- Oreopoulos L, Cahalan RF. 2005. Cloud inhomogeneity from MODIS. *J. Climate* **18**: 5110–5124.
- Oreopoulos L, Davies R. 1998. Plane parallel albedo biases from satellite observations. Part I: Dependence on resolution and other factors. *J. Climate* **11**(5): 919–932.
- Pincus R, Barker HW, Morcrette JJ. 2003. A fast, flexible, approximate technique for computing radiative transfer in inhomogeneous cloud fields. *J. Geophys. Res.* **108**(D13): 4376.
- Pincus R, Klein SA. 2000. Unresolved spatial variability and microphysical process rates in large-scale models. *J. Geophys. Res.* **105**(D22): 27 059–27 065.
- Räisänen P, Barker HW, Khairoutdinov MF, Li J, Randall DA. 2004. Stochastic generation of subgrid-scale cloudy columns for large-scale models. *Q. J. Roy. Meteorol. Soc.* **130**: 2047–2067.
- Ramaswamy V, Boucher O, Haigh J, Hauglustaine D, Haywood J, Myhre G, Nakajima T, Shi G, Solomon S. 2001. Radiative forcing of climate change. In: *Climate Change 2001: The Scientific Basis. Contribution of Working Group I to the Third Assessment Report of the Intergovernmental Panel on Climate Change*, Houghton J, Ding Y, Griggs D, Nougier M, van der Linden P, Dai X, Maskell K, Johnson C (eds), ch. 6, Cambridge University Press: Cambridge, United Kingdom and New York, USA, pp. 349–416.
- Rossow WB, Delo C, Cairns B. 2002. Implications of the observed mesoscale variations of clouds for the earth's radiation budget. *J. Climate* **15**(6): 557–585.
- Shonk JKP, Hogan RJ. 2008. Tripleclouds: An efficient method for representing horizontal cloud inhomogeneity in 1D radiation schemes by using three regions at each height. *J. Climate* **21**(11): 2352–2370.
- Shonk JKP, Hogan RJ. 2010. Effect of improving representation of horizontal and vertical cloud structure on the Earth's radiation budget. Part II: The global effects. *Q. J. Roy. Meteorol. Soc.* **136**: 1205–1215.
- Shonk JKP, Hogan RJ, Mace GG, Edwards JM. 2010. Effect of improving representation of horizontal and vertical cloud structure on the Earth's radiation budget. Part I: Review and parameterisation. *Q. J. Roy. Meteorol. Soc.* **136**: 1191–1204.
- Stephens GL, Vane DG, Tanelli S, Im E, Durden S, Rokey M, Reinke D, Partain P, Mace GG, Austin R, L'Ecuyer T, Haynes J, Lebsock M, Suzuki K, Waliser D, Wu D, Kay J, Gettelman A, Wang Z, Marchand R. 2008. CloudSat mission: Performance and early science after the first year of operation. *J. Geophys. Res.* **113**(D00A18).